

Distant Residues Modulate Conformational Opening in SARS-CoV-2 Spike Protein

Dhiman Ray^a, Ly Le^{a,b}, and Ioan Andricioaei^{a,c,1}

^aDepartment of Chemistry, University of California Irvine, Irvine CA 92697; ^bSchool of Biotechnology, International University, Vietnam National University, Ho Chi Minh City, Vietnam; ^cDepartment of Physics and Astronomy, University of California Irvine, Irvine CA 92697

1 Infection by SARS-CoV-2 involves the attachment of the receptor
2 binding domain (RBD) of its spike proteins to the ACE2 receptors
3 on the peripheral membrane of host cells. Binding is initiated by a
4 down-to-up conformational change in the spike protein, the change
5 that presents the RBD to the receptor. To date, computational and
6 experimental studies that search for therapeutics have concentrated,
7 for good reason, on the RBD. However, the RBD region is highly
8 prone to mutations, and is therefore a hotspot for drug resistance.
9 In contrast, we here focus on the correlations between the RBD and
10 residues distant to it in the spike protein. This allows for a deeper
11 understanding of the underlying molecular recognition events and
12 prediction of the highest-effect key mutations in distant, allosteric
13 sites, with implications for therapeutics. Also, these sites can ap-
14 pear in emerging mutants with possibly higher transmissibility and
15 virulence, and pre-identifying them can give clues for designing pan-
16 coronavirus vaccines against future outbreaks. Our model, based
17 on time-lagged independent component analysis (tICA) and protein
18 graph connectivity network, is able to identify multiple residues that
19 exhibit long-distance coupling with the RBD opening. Residues in-
20 volved in the most ubiquitous D614G mutation and the A570D muta-
21 tion of the highly contagious UK SARS-CoV-2 variant are predicted
22 *ab-initio* from our model. Conversely, broad spectrum therapeutics
23 like drugs and monoclonal antibodies can target these key distant-
24 but-conserved regions of the spike protein.

Molecular biophysics | molecular dynamics | virus structure | statistical
mechanics | computer simulation of proteins | COVID-19

1 The COVID-19 pandemic continues its spread, with more
2 than 160 million confirmed cases worldwide, including 4.1
3 million deaths by the end of July 2021, according to the World
4 Health Organization. The etiological agent, SARS-CoV-2, is
5 a member of the *Coronaviridae* family, which includes SARS-
6 CoV-1 (2002-2004) and MERS-CoV (since 2012), viruses with
7 which SARS-CoV-2 has a sequence identity of 79.6% and 50%,
8 respectively (1, 2). Expressed on the surface of SARS-CoV-2,
9 the spike (S) protein plays a crucial role in infection. It binds
10 to the host angiotensin-converting enzyme 2 (ACE2) through
11 the S protein's receptor-binding domain (RBD), thereby fa-
12 cilitating viral entry into host cells (3, 4). Therefore, the
13 spike protein is a preponderant target for inhibitors that im-
14 pede SARS-CoV-2 infection. Assessing the genomic variability
15 of SARS-CoV-2 reveals a moderate mutation rate compared
16 to other RNA viruses, around 1.12×10^{-3} nucleotide sub-
17 stitutions/site/year (5), (but much larger than DNA viruses
18 (6)); the SARS-CoV-2 mutation rate is at the same level as
19 SARS-CoV-1 (7). Significantly, the spike protein has been
20 demonstrated to be particularly susceptible to acquiring muta-
21 tions (5, 8-10). More specifically, a study analyzing 10,022
22 SARS-CoV-2 genomes from 68 countries revealed 2969 differ-
23 ent missense variants, with 427 variants in the S protein alone

24 (5). This suggests a strong propensity to form new strains
25 with higher virulence and more complicated epidemiology;
26 the dominant D614G mutation and the recent B.1.1.7 mu-
27 tant are notable examples (11). Spike protein variability can
28 thus render currently existing therapeutic agents ineffective in
29 combating SARS-CoV-2 and other probable SARS epidemics
30 in the future. It therefore is of fundamental value to under-
31 stand, in microscopic detail, the role of spike mutations to the
32 structural dynamics that triggers infection.

33 Large scale screening of therapeutic molecules and anti-
34 bodies are underway, aiming to target the spike protein and
35 consequently to prevent infection. Most of the experimental
36 (12-15) and computational (16-18) efforts for inhibitor design
37 focus on the receptor binding domain (RBD), despite the fact
38 that this region is highly mutation-prone (see, for example,
39 Verkhivker (19), Spinello et al. (20) and our own sequence
40 alignment study in the SI Appendix) and can cause resistance
41 to therapeutics. For instance, the mutations in the RBD ob-
42 served in the emerging viral lineage in South Africa resulted
43 in up to a ten-fold reduction in the neutralization capacity of
44 conventional antibody therapy (21).

45 However, domains in the spike other than the RBD are also
46 possible targets for inhibition. The human immune system
47 started generating antibodies specific to residues outside the
48 RBD even at the early stages of the pandemic. Liu et al.
49 extracted, from infected patients, multiple COVID-19 neutral-
50 izing antibodies, a fraction of which bind to non-RBD epitopes
51 of the S-protein, such as the N-terminal domain (NTD) (22).
52 Moreover, a separate group of antibodies, present in the blood-
53 stream of uninfected humans (particularly, and importantly,

Significance Statement

The novel coronavirus (SARS-CoV-2) pandemic resulted in the largest public health crisis in recent times. Significant drug design effort against SARS-CoV-2 is focused on the receptor binding domain (RBD) of the spike protein, although this region is highly prone to mutations causing therapeutic resistance. We applied deep data analysis methods on all-atom molecular dynamics simulations to identify key non-RBD residues that play a crucial role in spike-receptor binding and infection. Because the non-RBD residues are typically conserved across multiple coronaviruses, they can be targeted by broad spectrum antibodies and drugs to treat infections from new strains that might appear during future epidemics.

DR designed research with inputs from LL and IA. DR performed MD simulations and analyzed results. LL performed and analyzed sequence alignment. DR, LL and IA wrote the paper.

The authors declare no competing financial interest.

¹To whom correspondence should be addressed. E-mail: andricio@uci.edu

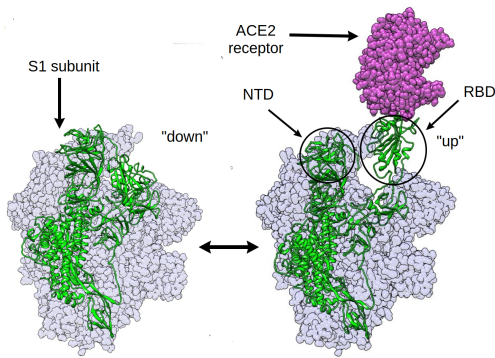


Fig. 1. The RBD opening transition in the SARS-CoV-2 spike protein: the RBD of the chain shown in green is undergoing the *down* to *up* transition leading to the binding of the human ACE2 receptor.

54 in children), were observed to bind specifically to the S2-stem
55 region. This structure has virtually identical sequence in all
56 coronavirus strains, including the ones causing common cold
57 (23). It is the presence of such universal antibodies, selective
58 to the conserved regions of the spike, that is hypothesized to
59 cause the absence of severe infections in children. These obser-
60 vations motivate an effort towards designing small-molecule
61 drugs and antibodies targeted towards residues far from the
62 RBD in the 3D structure which, consequently, are less prone
63 to mutation.

64 A number of studies explored druggable hotspots in the
65 spike protein that modulate, via allostery, ACE2 binding
66 (20, 24–26). A concurrent computational study established
67 that RBD mutations appearing in the new strains of SARS-
68 CoV-2 can, via allosteric effects, increase binding affinity of
69 the spike to the human ACE2 receptor as well as impair the
70 binding interactions of neutralizing antibodies (20). Hydrogen
71 deuterium exchange mass spectrometry (HDXMS) experiments
72 revealed the dampening and the increase of conformational
73 motion at the stalk region and the proteolytic cleavage site
74 respectively, upon RBD binding to the ACE2 receptor (26).
75 Although this is a noteworthy approach towards targeting
76 non-RBD residues, the S-ACE2 bound complex, once formed,
77 already can initiate infection. So inhibitors which bind to the
78 ACE2-bound spike are only partially effective in preventing
79 viral entry. We, therefore, focus our study on the effect of
80 distant residues on the dynamics of the structural transition
81 in the spike protein leading to the RBD-up conformation,
82 i.e., before it becomes poised for binding (see Fig 1). This is
83 because RBD opening plays an obligatory role in the infection
84 by displaying the RBD to the ACE2 receptor. (27–31).
85 Therapeutics inhibiting this structural transition can therefore
86 prevent ACE2 binding altogether, providing a higher degree
87 of barrier towards the infection.

88 The down-to-up transition of the S-protein RBD has been
89 subjected to extensive cryogenic electron microscopy (cryo-
90 EM) studies that elucidated the atomic resolution structures
91 of the closed (PDB ID: 6VXX (32), 6XR8 (33)), partially
92 open (PDB ID: 6VSB (34)) and fully open (PDB ID: 6VYB
93 (32)) states. Attempts have been made to study the dynamics
94 of RBD opening using force-field based classical molecular
95 dynamics (MD) simulation (35, 36). However, the direct ob-
96 servation of an RBD opening transition is beyond the scope of
97 atomistic MD simulation, primarily because of the large size of

the system and the long timescales involved. Yet, combining
multiple short trajectories totaling up to 1.03 ms, the Fold-
ing@Home project could resolve various intermediates of the
RBD opening transition (36). Alternatively, Gur et al. used
steered molecular dynamics in combination with unbiased MD
simulations to uncover the mechanism of the conformational
opening process (30). They obtained a free energy landscape
and delineated the effect of salt bridges on the transition.
Moreover, structure-based coarse-grained modeling could be
employed to explore the conformational landscape of multiple
configurations of the spike trimer (1-up-2-down, 2-up-1-down,
3-up and 3-down) (37), and, in a separate study, to iden-
tify allosteric communication pathways in the spike protein
(19). Despite providing qualitative insight, the absence of
explicit solvent and atomistic detail and the exclusion of the
glycan-shield (which plays dynamic roles beyond shielding
itself (35, 38)) obscured a quantitative mechanistic picture of
the conformational opening transition.

We took a three-pronged approach to identify the distant
residues that show correlated motion coupled to RBD opening
and closing. First, as an initial exploration, we pulled the
RBD of the closed state at non-equilibrium, to generate a
putative open structure. Using potential of mean force (PMF)
calculations, obtaining a non-equilibrium work profile, this
structure, as expected, lead to a value higher than the equi-
librium free energy (20 kcal/mol, see Fig S1 in SI Appendix).
This is akin to a single-molecule pulling experiment (39). How-
ever, we emphasize that we do not use the reaction coordinate
(RC) to derive any quantitative data. Given the artificiality of
the result obtained by following a single degree of freedom, we
resorted to the use of the more sophisticated tICA coordinates
to capture the motion. We then designed and employed a
novel way to identify residues important for the conformational
change by quantifying the correlation of the backbone torsion
angles of the protein with the slowest degrees of freedom,
representing the down-to-up transition of the RBD. Thirdly,
we took an alternative route to study allosteric connections
by constructing a protein graph connectivity network model
that uses the mutual information metric computed from MD
trajectories. Taken together, the three approaches resulted in
the prediction of a handful of residues in non-RBD regions of
the S protein that play a crucial role in the conformational
rearrangements of the spike. These residues suggest possible
future mutational hotspots, as well as targets for designing
inhibitors that can reduce the flexibility of the RBD, leading
to reduced receptor binding capability. In fact, the most ubiq-
uitous spike protein mutation to date, the D614G (40), and
the A570D mutation in the recently emerged highly conta-
gious UK SARS-CoV-2 strain (41), both appeared among our
predicted set of residues, the latter having been discovered
after the completion of our calculations.

Results

**Correlation between RBD-opening and backbone dihedral an-
gle.** Multiple unbiased trajectories were propagated from dif-
ferent regions of the S-protein RBD-opening conformational
space, priorly explored by steered MD and umbrella sampling
(details in Supporting Information (SI) Appendix). Three of
those trajectories were assigned as the closed, partially open,
and fully open state, based on the position of free energy
minima along the umbrella sampling reaction coordinate (cf.

Fig. S1 in SI Appendix). The stability of these three conformations were ensured by inspection of the trajectories. The cumulative simulation data was projected onto a feature space composed of pairwise distances between residues from RBD and from other parts of the spike near the RBD (details in SI Appendix); these distances increase during the down-to-up transition. The projected trajectory data were subjected to principal component analysis (PCA) (42) and time-lagged independent component analysis (tICA) (43–45). The former method calculates the degrees of freedom with the highest variance in the system, while the latter obtains the ones with the longest timescale. These methods quantify large conformational changes in complex bio-molecules. The goal of performing PCA and tICA is to find out one or two coordinates which best describe the RBD opening motion. As one continuous trajectory hardly samples the transition event, multiple short trajectories spanning a large range of the configuration space were used (46).

The first principal component (PC) and the first time-lagged independent component (tIC), obtained from PCA and, respectively, from tICA analysis could both distinguish the closed and open states, although the partially open and fully open states could not be distinguished within the first two PCs (Fig. S2 in SI Appendix). Yet, the projections of the open- and closed-state trajectories along the first two principal components are in agreement with the results of previous long multi-microsecond spike protein simulations (35). Because of the clear distinction between the closed, open and the intermediate, partially open states (Fig. 2b), we chose the first two time-lagged independent components (tICs) for our subsequent analysis.

Large scale conformational changes in proteins are, at a fundamental level, stemming from complex combinations of transitions between various states of the protein-backbone torsional angles ϕ and ψ . These combinations add up to global displacements, which set the timescale for internal friction (47) and gauge the paradoxically large number of conformational states accessible to a protein as it folds (48). On one hand, concerted transitions of the backbone torsions typically lead to large scale motion. On the other hand, exponential divergence in nonlinear dynamical systems (49) is such that only certain dihedrals are likely to predominantly effect the conformational changes. We therefore hypothesize that there exist specific residues in the spike protein, for which the transition in backbone dihedral states result in the opening of the RBD. Moreover, we conjecture that, given the significant mutation rate, and because of the selection pressure on the virus, the residues with large impact in collective motions that facilitate infectivity are likely to be selected in spike mutants. To test this hypothesis we calculated the Pearson correlation coefficients of the sines and cosines of all the ϕ and ψ backbone torsion angles of all the residues with the first two tICs. The magnitude of the correlation is found to be significantly large only for a handful of torsion angles, whereas the majority show near-zero correlation (Fig. S3 in SI Appendix).

We defined a metric called “correlation score” (CS) for each torsion angle in each residue. The value of the metric is computed as:

$$CS(\theta) = |C(\cos(\theta), \mathbf{IC1})| + |C(\sin(\theta), \mathbf{IC1})| + |C(\cos(\theta), \mathbf{IC2})| + |C(\sin(\theta), \mathbf{IC2})| \quad [1]$$

where θ , $\mathbf{IC1}$ and $\mathbf{IC2}$ are the vectors containing the time series of the angle θ , the tIC1 and tIC2 respectively, and $C(\mathbf{x}, \mathbf{y})$ is the Pearson correlation coefficient of datasets \mathbf{x} and \mathbf{y} . The CS metric can take values from 0 to 4 and a higher value indicates that the particular torsion angle shows a highly correlated (or anticorrelated) motion with the slowest conformational change which in this case the RBD transition. We avoided summing over the Φ and Ψ angles of the same residue, or over residues of different protein chains as it might average out the contributions from each angle and consequently obscure the process of specifying the role of each individual residue in the conformational transition.

We sorted the residues based on the CS scores of their torsion angles and a list is provided in the SI. The highest values of correlation scores are shown primarily by pairs of consecutive residues, with ψ of the first and the ϕ of the second residue, as depicted in Table 1. This suggests that two consecutive torsion angles in certain regions of the protein are highest correlated with the RBD opening motion. Most dihedrals belonged to residues in the loop structure joining the RBD with the S2 stem, as this region is a hinge for the opening of the RBD. This correlation does not exclude causation, since change in the conformational state for two subsequent torsion angles can induce crankshaft motion (50) in the backbone which, propagating along the chains, leads to a change in protein structure.

The distribution of some of the dihedral angles, with highest CS scores, in the closed and partially open states, are depicted in Fig. 2d. Similar plots for all torsion angles with $CS > 2.0$ are provided in the SI Appendix. We compared the dihedral angle distribution only between the closed and the open states as the significance of the artificially prepared fully open structure should not be overemphasized. This structure, generated from the closed state using steered molecular dynamics and umbrella sampling (see SI Appendix), is only an approximation for a more exact RBD up structure that binds the ACE2 receptor. In literature the structure with PDB ID: 6VSB is sometimes referred to as the open conformation (35), which, in this work, we refer to as the “partially open” state. So, in the rest of the paper, when we attempt to compare the behaviour of a chosen set of residues between closed and open states at an atomistic detail, we only include the closed and partially open configurations.

The fact, that the highly correlated residues follow a distinctly different distribution in the backbone torsion angle space (Fig 2d), indicates that a handful of non-RBD residues can play a pertinent role in the conformational change of the spike and, consequently, in the viral infection. Interestingly, the correlated torsion angles span over all three chains of the spike trimer, namely A (the one undergoing the RBD transition), B and C (Fig. 2a and Table 1), hinting at the potential role of inter-residue couplings ranging over long distances in presenting the RBD to the ACE2 receptor. The residues exhibiting highest correlation scores (Table 1), particularly Gln613, Asp614, Pro600, Gly601, Ile569 and Ala570, are present in the linker region joining the RBD with the S2 domain, which, as mentioned above, is the hinge for the opening motion that presents the RBD to the receptor (51). The Phe833 and Ile834 residues, although technically part of S2 domain, can significant impact the dynamics of the hinge or linker due to their proximity in 3D structure. Similar ar-

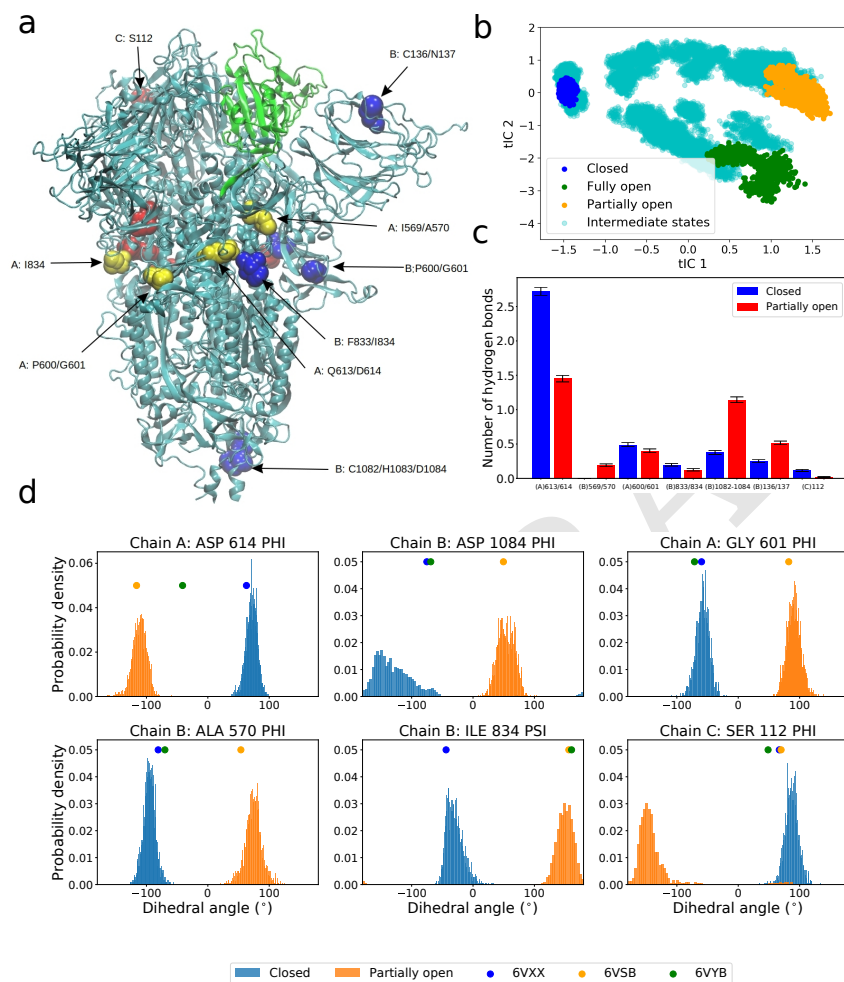


Fig. 2. (a) Structure of spike protein with the residues in RBD shown in green color. Non-RBD residues strongly correlated with the RBD opening motion are represented by spheres (color code: chain A: yellow, chain B: blue, chain C: red). The RBD of chain A is performing *down-to-up* conformational change. (b) The projection of all unbiased trajectories along the two slowest degrees of freedom (tICs) obtained from tICA analysis. (c) Average number of hydrogen bonds for the highest correlated residues/residue-pairs (Table 1) in the closed and the partially open state. (d) Normalized distribution of representative backbone dihedral angles strongly correlated with tIC 1 and tIC 2 (Table 1). The distributions are calculated from closed and partially open state trajectories. The corresponding values of the dihedral angles in the PDB structures are marked in the plot for reference.

guments are applicable for the NTD domain residues such as Cys136 and Asn137 from chain B and Ser112 from chain C, which are able to impact the RBD due to their structural proximity. Interestingly, residues near the stem region, including Cys1082, His1083, and Asp1084 appear in our list as strongly correlated and can potentially be used as a target for broad spectrum antibody or vaccine design targeting the stem region (52, 53).

When the virus mutates these particular residues in a way that increases its virulence, this increase stems from the propensity of the RBD to “flip” open and thereby increase ACE2 binding. As evidence, we highlight the example of the D614G mutation, which is already observed in numerous strains of the SARS-CoV-2 all over the world (10, 40). Cryo-EM studies have indicated that the D614G mutation is, by itself, capable of altering the the conformational dynamics of spike protein by stabilizing a RBD up state over the down conformation (54, 55). D614 is one of the top ranked residues predicted from our model for the potential to play a crucial role in RBD opening. A glycine residue has the least backbone-torsion barrier for conformational transition in ϕ - ψ space due to the absence of a side chain. Replacing an Asp residue, which has higher barriers to such transitions, with a glycine can increase the flexibility of the backbone, significantly impacting the probability of observing an RBD-up conformation. **To understand if this can be the reason why this particular mutation was selected to become so widespread, a comparison of the geometric and "chemical" effects of Gly should be assessed. To this end, we performed additional simulations of the open and closed states of the D614G mutant. Indeed, our simulations of the D614G mutant spike indicate that, unlike the wild type system for which a significantly different dihedral angle distribution exists, there is no difference between the closed and the partially open configuration in terms of the torsion angle space explored by residue G614 (see Fig. S14 in SI Appendix). The glycine residue at 614 position also experienced different degrees of hydrogen bonding and electrostatic interactions (see below).**

A wide range of spike protein mutant sequences have been characterized, each with varying degrees of abundance. A relatively rare mutation, A570V, resulted in a decrease of the overall stability of the spike protein in all three states, based on the FoldX empirical force field (10, 56). Free energy values (10) were obtained from only structural data and no dynamical information was considered in that study. Yet it is worth noting that the change in total and solvation free energies, due to this mutation, were substantially different for the closed and open states, resulting in a change in ΔG for RBD opening. But, as the side chains of Ala and Val are similar in terms of steric bulk, this mutation is unlikely to significantly impact RBD dynamics. As it likely did not increase the evolutionary advantage of the virus by increasing infectivity, this mutation, only occurring in one strain (10) so far, did not become as prevalent as D614G.

On the contrary, a A570D mutation is observed in the same residue in the newly emerged and highly infectious B.1.1.7 strain in the UK (41, 57, 58). This mutation is likely to play a pertinent role in infection as it replaces a hydrophobic amino acid with a charged one. This leads to a significant difference in the conformational dynamics of the 570 residue and consequently impacts the large scale RBD opening mo-

tion. Structural biology experiments have established that a mutation in the A570 residue alters the propensity of RBD opening by modulating the hydrophobic interaction of the hinge region with the S2 core (59). Coarse grained modeling studies explained this observation by noting that A570 is part of a regulatory switch that triggers the conformational change necessary for receptor binding (60).

The B.1.1.7 also shows a P681H mutation close to the highly correlated N679 residue predicted from our model (see Fig. S5 in SI Appendix). As this mutation replaces a structurally rigid proline residue, it can possibly impact the conformational space accessible to nearby residues, including N679.

Giving pause for thought, these results indicate that mutations in the highest correlated residues (Table 1) can in fact have significant physiological impact in changing the course of the pandemic. Therefore, we provide a list of residues (Table 1 and Fig. S3-S10 in SI Appendix), future mutations of which could impact RBD dynamics and consequently change the transmissibility or virulence of SARS-CoV-2. (See data availability statement for access to the raw correlation coefficient data for all residues.) Yet, care should be taken with assigning the predominant role in infection to a single, non-RBD domain residue in the UK variant; several other mutations are present that could modulate the binding affinity to the ACE2 receptor (particularly N501Y in the RBD-ACE2 binding interface). However, mutations outside the RBD can indeed play a key role in infection by disproportionately favoring an RBD “up” structure (52, 53, 59).

For a more detailed understanding we compared the average number of hydrogen bonds per residue group from Table 1 for the closed and the partially open trajectory (Fig 2c). We observed significant changes in the number of hydrogen bonds in residue groups: Q613/D614, I569/A570, C1082/H1083/D1084, and C136/N137 (Fig. 3). In the closed state, the carboxylate side-chain of D614 residue forms hydrogen bonds with K854 and T859 which are lost in the RBD up configuration. These hydrogen bonds will be absent in D614G mutant and likely reduce the energy cost of the conformational transition. Particularly the loss of hydrogen bond with T859 has been attributed to the higher stability of the RBD up structure in D614G mutant by Mansbach et al. (61). **Our simulations also indicate that there is a loss of one hydrogen bond in the Q613/D614 residues going from RBD down to RBD up conformation in the WT spike. But such loss of hydrogen bonding is not observed in case of D614G mutant (see SI Appendix).** On the contrary, formation of new hydrogen bonds are observed in the other three residue groups (Fig. 3) which can be enhanced or reduced by mutating the residues involved.

Additionally, the non-bonded interaction energies (electrostatic and van der Waals (vdW)) of the residues, from Table 1, differ significantly in the two conformations. Unsurprisingly, the D614 is energetically stabilized in the closed conformation in comparison to the open state due to additional hydrogen bonds. **In the D614G mutant, from our analysis, this stabilization is significantly lower in comparison to the WT (see Fig. S15 and discussion in SI Appendix.)** But residues P600/G601 are more stabilized in the open state in comparison to the closed state via favourable Coulomb and vdW interactions. Similar effect is observed in C136 for electrostatic energy but is somewhat compensated for by the opposite trend in vdW energy. A570 and N137 have lower electrostatic energy in

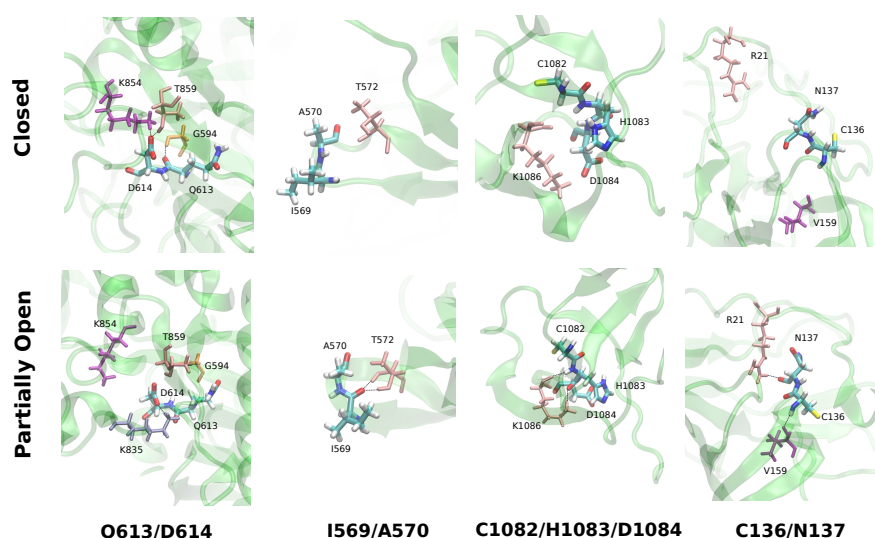


Fig. 3. Representative snapshots of the hydrogen bonding pattern of some of the groups of residues from Table 1 and Fig. 1c. The upper panel corresponds to the closed state and the lower panel shows the partially open state.

400 the closed state despite having fewer hydrogen bonds. In
 401 short, non-RDB residues that experience different amount of
 402 non-bonded interaction with the rest of the protein or show
 403 different hydrogen bonding patterns in the “RBD down” and
 404 “RBD up” state, can impact the relative stability of those
 405 two conformations when mutated into residues with different
 406 properties.

Table 1. A list of residues for which the backbone torsional angles are strongly correlated with the first two tIC components. The correlation score for each of the dihedral angles (see text and SI Appendix) is also reported.

Residue	Chain	Predominant angle	Correlation score (<i>CS</i>)
Gln613	A, B, C	ψ	2.62, 2.61, 2.59
Asp614	A, B, C	ϕ	2.56, 2.54, 2.46
Cys1082	B	ϕ	2.25
His1083	B	ψ	2.54
Asp1084	B	ϕ	2.49
Pro600	A, B, C	ψ	1.56, 1.48, 1.52
Gly601	A, B, C	ϕ	2.37, 2.31, 2.33
Ile569	A, B, C	ψ	2.40, 2.49, 2.46
Ala570	A, B, C	ϕ	1.56, 2.22, 2.16
Cys136	B	ψ	1.42
Asn137	B	ψ, ϕ	1.70, 1.80
Phe833	B	ψ	2.37
Ile834	A, B, C	ψ	1.73, 2.40, 2.12
	A	ϕ	1.19
Ser112	C	ψ, ϕ	1.67, 2.23

407 **Mutual information and network model.** A different approach
 408 to characterize the coupling between distant regions in a pro-
 409 tein is to calculate the cross correlations between the posi-
 410 tions of different residues in 3D space. This method is often
 411 used to study allosteric effects upon ligand binding (62–67).
 412 Conventional implementations compute the dynamic cross
 413 correlation map (DCCM) of the position vectors of the C_α
 414 atoms (68). However, DCCM ignores correlated motions in
 415 orthogonal directions (67). This problem can be avoided by us-
 416 ing a linear mutual information (LMI) based cross-correlation
 417 metric, which we use in the current study (62, 69). The

cross-correlation matrix elements, C_{ij} , are given by

$$C_{ij} = (1 - e^{-(2/d)I_{ij}})^{-1/2}, \quad [2]$$

where I_{ij} is the linear mutual information computed as

$$I_{ij} = H_i + H_j - H_{ij} \quad [3]$$

with H the Shannon entropy function:

$$H_i = - \int p(\mathbf{x}_i) \ln p(\mathbf{x}_i) d\mathbf{x}_i$$

$$H_{ij} = - \int \int p(\mathbf{x}_i, \mathbf{x}_j) \ln p(\mathbf{x}_i, \mathbf{x}_j) d\mathbf{x}_i d\mathbf{x}_j, \quad [4]$$

where, for two residues i and j , $\mathbf{x}_i, \mathbf{x}_j$ are the 3-dimensional
 Cartesian vectors of atomic coordinates of the corresponding
 C_α atom, whereas $p(\mathbf{x}_i)$ and $p(\mathbf{x}_i, \mathbf{x}_j)$ indicate, respectively,
 the marginal probability density for \mathbf{x}_i and the joint probability
 density of \mathbf{x}_i and \mathbf{x}_j (62, 69).

The change in cross-correlation between the apo and holo
 states of a protein is a gauge that traces allosteric communi-
 cation in the protein by monitoring the changes in the local
 correlations between protein residues(62). The spike protein
 conformational change is not an allosteric process by strict
 definition as it does not involve the binding of an effector. But
 comparing the LMI cross correlations between the RBD-down
 and up states can help identify residues which behave differ-
 ently in different protein conformations. More importantly
 the difference of correlation between the closed state and a
 small perturbed structure towards the conformational opening,
 can hint at the residues which gain or loose contact in the
 beginning stage of the opening transition and consequently
 initiating the large scale motion. So we assigned one of the
 unbiased trajectories as "slightly open", indicative of an early
 stage structure in the pathway of opening. We included the
 unbiased trajectory, corresponding to this structure, in our
 subsequent analysis, in which we compared the correlation
 heat map of all residues in the closed form with the three
 open states, namely the partially open, fully open, and slightly
 open state, in order to understand the coupling between RBD
 opening and protein residue fluctuations.

Overall change in LMI correlation is clearly larger for the
 fully open state in comparison to the partially open state as

evident from the higher appearance of reddish color (Fig. 4 a-d). Unsurprisingly, the change is largest for the RBD and proximal residues encompassing the N-terminal domain region (residue 100-300) in all chains (Fig. 4 bottom panels), as they loose direct contact during the opening motion. Residues in the RBD-S2 linker region in Chain A and C (residue 524-700) show a large gain in correlation in the initial stage of RBD opening (“slightly open”) despite being not directly in contact with the RBD in the closed form. **On the pathway from close to open, relevant correlation changes are already found in the slightly-open state when comparing to the closed state (Fig. 4e), with significant changes for the important RBD-S2 linker region. However, more details appear (in other distant regions) as the transition approaches the partially-open and fully open states, cf. Fig 4f-g.**

Overall these results are consistent with the dihedral angle correlations, described in the previous section: the residues in the loop region next to the RBD exhibit a change in the values of the backbone dihedral angles upon the down-to-up transition. The change in the correlation coefficient (Δ Correlation) is also large for the RBDs and NTDs of chain B and C, which are in close proximity to chain A of the RBD in the closed state. Additionally, linker residues of chain B show significant gain in correlation upon the transitioning to the fully open state. Some residues that gain or loose correlation (blue or red coloration in Fig. 4 bottom panels) are situated at the opposite end (S2 region) of the spike, indicating the presence of long range correlated motion. This long-distance correlation can indeed be a cumulative effect of many small local fluctuations on the way towards the RBD, along structural patches connecting these sites, allowing "distant" residues to shed their impact on the structural transition in RBD. These pathways can be revealed, for example by the method of Ota and Agard (70), who used energy flow or vibrational energy relaxation to trace them.

For a more profound insight, we built a protein connectivity graph network-model. In it, the C_{α} atoms of each amino acid are the nodes and the correlation between them are the edges connecting the nodes. The number of nodes in our system is $N=3438$, which makes it one of the largest systems studied previously with this method (62–67)(Comparable to the work by Saltalamacchia et al. on a spliceosome complex involving 4804 C_{α} atoms and 270 phosphorus atoms in the network (71)). We then calculated the betweenness centrality (BC), a graph theoretical measure that provides a way to quantify the amount of information that flows via the nodes and edges of a network. If a node i is working as a bridge between two other nodes along the shortest path joining them, then the BC of node i is given by

$$BC(i) = \sum_{st} \frac{n_{st}^i}{g_{st}}, \quad [5]$$

where g_{st} is the total number of geodesics (shortest paths) joining nodes s and t , out of which n_{st}^i paths pass through node i (63). The change of BC in the dynamics of the spike protein has been recently observed using coarse-grained simulation methods(19). Despite the coarseness of the model, a handful of residues participating in the information-propagating pathway could be identified directly from the BC values. In the current work, we used the difference in BC as a metric to identify key residues which gain or loose relative importance

along the allosteric information pathway. The difference in the normalized BC is measured by comparing the number for the partially open and fully open states with the closed conformation (i.e. $BC^{\text{slightly open}} - BC^{\text{closed}}$, $BC^{\text{partially open}} - BC^{\text{closed}}$ and $BC^{\text{fully open}} - BC^{\text{closed}}$ for every residue in the spike protein) from our all atom trajectories with explicit solvation. Importantly, our model also includes the highly relevant glycan shield, which were shown to modulate the conformational dynamics of the RBD by favoring a *down* conformation and functioning as a gate for the conformational opening, beyond their general role in shielding (35, 38). However, glycans were not included in the network analysis. While in principle it is valid to consider their role, their motion occurs on time scales that are much faster than those of the protein backbone and would be averaged out of any correlation calculation.

For slightly open, partially open and fully open states, the residues with significant (e.g., >0.1) change in BC are mostly from the NTD region or RBD region of the B and C chain (Figs. 5 and 6). This suggests that the allosteric information flows through the nearby NTD's and RBDs, and mutations in this region can break the allosteric network (63) and affect the functionality of the spike protein. SARS-CoV-2 neutralizing antibodies were indeed observed to bind these regions of the spike (22). The identified residues are in close proximity to the RBD of chain A, the one undergoing the *down* to *up* transition.

So the connectivity captured in the BC data is primarily due to short-range coupled fluctuations. Such couplings are broken when the RBD and NTD move apart, leading to the change in BC. For the same reason, the BC of the RBD of chain A increases in the fully open state as its internal vibrations become more independent of the rest of the protein.

In a culmination of the above, the most interesting aspect is the strikingly large change in BC of the residues which are *distant* from the RBD in 3D structure. Significant gain or loss of BC is observed in residues 607, 624, 713, 757, 896, and 1097. The first three residues are present in the linker region joining the RBD with the S2 domain, while the other three are in the S2 itself. The linker region has a strong impact on the dynamics of the RBD as we already established from the dihedral angle analysis. The allosteric network analysis reinforces this conclusion. Moreover, the large change of BC in the S2 domain indicates a complex long-range information flow connecting the RBD with the core residues of the protein. Electrostatic and van der Waals energy analysis, similar to that mentioned in the previous section, has been performed on the residues with changes in BC greater than 0.2. The interaction energy of the S2 domain residues such as I896 and G757 are significantly different for the closed and open state along some of the NTD residues like N188, V6, and S98. This has substantial implications for pharmaceutical design, as mutations within the NTD and the S2 domain can impact the receptor-binding propensity of the viral spike. These results also suggest that therapeutics targeted towards the S2 and towards the RBD-S2 linker can be effective in preventing COVID-19 infection, without complications stemming from the high rate of mutations in the RBD.

Concluding Discussion

To tame the raging pandemic, we need to be able to control the fundamental dynamics of the spike protein. Its motion is key to the infection machinery of the SARS-CoV-2 virus.

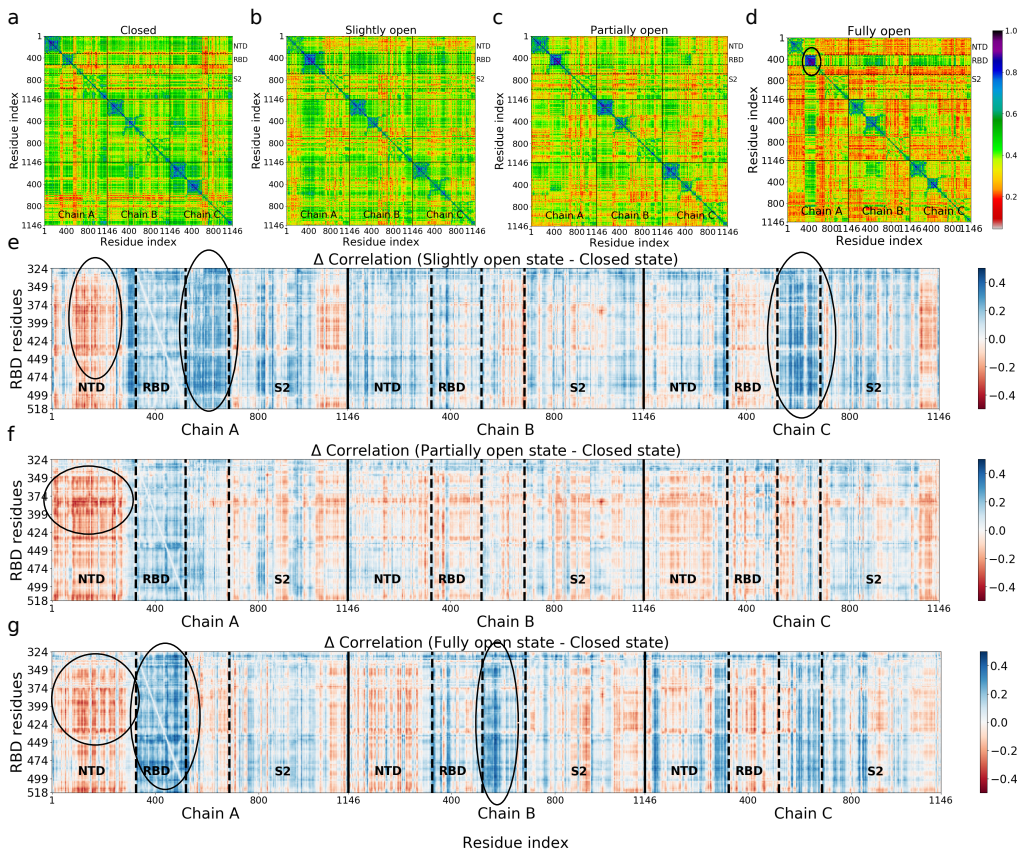


Fig. 4. Upper panel: Cross correlation matrices for four states (a: closed, b: slightly open, c: partially open, d: fully open) computed using linear mutual information (LMI). Lower panel: Difference in correlation matrix elements for the (e) slightly, (f) partially and (g) fully open states with respect to the closed state. RBD regions form highly correlated blocks (d,g), indicating that these residues are largely decoupled from the rest of the protein. Still, signatures of long-distance correlated motion are detectable.

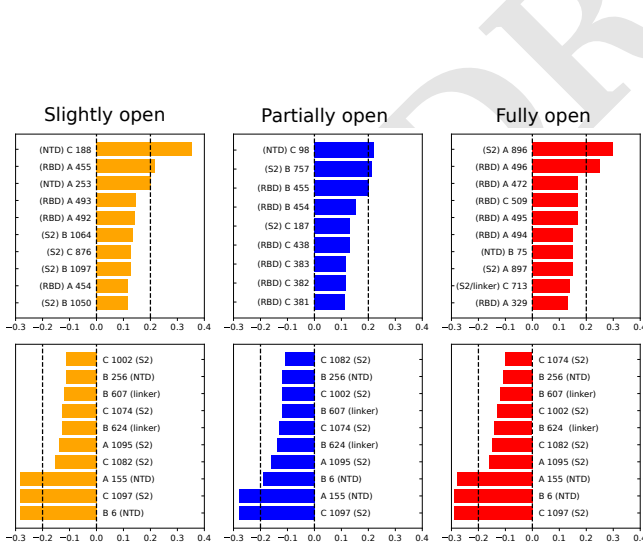


Fig. 5. Residues with large changes in normalized betweenness centrality (BC) due to RBD opening. Upper panel: largest positive changes; lower panel: negative changes; chain index (A,B, or C) mentioned before the residue number. The location of the residue (NTD, RBD, linker or S2) is also mentioned next to the residue number.

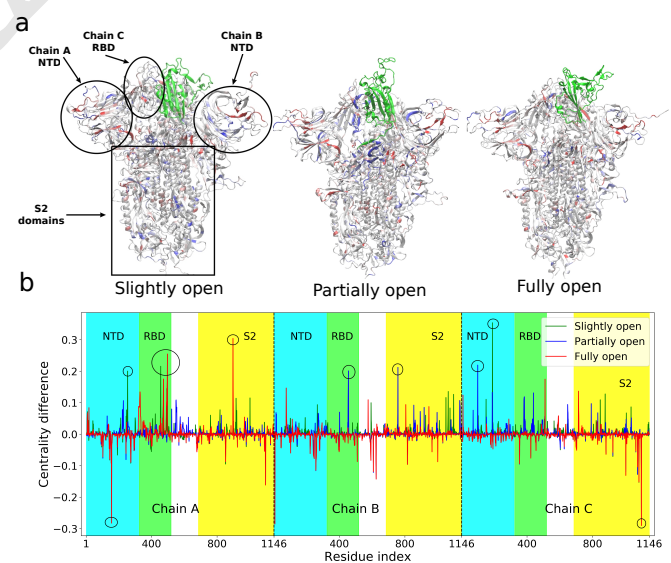


Fig. 6. (a) Structures of the slightly open, partially open and the fully open states of the spike protein with residues colored according to the difference of betweenness centrality (BC) with respect to the closed conformation. Red indicates most negative and blue most positive values of BC difference. The RBD of chain A that undergoes opening motion is colored in green. The NTD and S2 domains are also indicated. (b) The values of the difference in centrality with respect to closed state plotted as a function of residue indices. Residues with BC difference > 0.2 marked with circle.

572 By understanding the role of residues in its structure, we
573 can anticipate the effect of new mutations and customize
574 treatments ahead of time. To curb the negative impact of rapid
575 mutations, we here focused on the allosteric effect of protein
576 residues that are *away* from its rapidly-mutating epitope (the
577 RBD) on the conformational change needed for infection.

578 We performed molecular dynamics simulations, with un-
579 supervised machine learning (tICA) and graph theory-based
580 analysis to identify the role of physically distant residues in the
581 dynamics of the receptor binding domain in the SARS-CoV-2
582 spike protein. We correlated the protein backbone torsion
583 angles with the slowest degrees of freedom encompassing the
584 structural transition of the receptor binding domain. With this
585 approach we were able to elucidate a small number of distant
586 non-RBD residues which strongly influence the conformational
587 change of the spike, change that in turn leads to binding to
588 the ACE2 receptor and then to infection. Residues in the
589 linker between the RBD and the S2 stem work as a hinge by
590 driving the down-to-up RBD transition via backbone torsional
591 changes. Out of the most correlated residues, D614 ranks
592 close to the top. The D614G mutation is currently observed
593 in SARS-CoV-2, and is becoming widespread among infected
594 patients throughout the world. In vitro experiments also es-
595 tablished that the single point mutation D614G is capable of
596 altering the “down” to “up” conformational dynamics of the
597 sike (55). The D614G mutant prefers the one RBD “up” state
598 ~7 times more than the “3-down” configuration while they
599 are equally likely in the wild type strain (54). The specific
600 role of the D614G mutation was recently also established by
601 coarse grained MD study(72). Our model predicted the D614
602 residue as a key player in RBD dynamics from physics-based
603 atomistic simulations without any prior knowledge of the mu-
604 tation profile of the spike. With glycine being more flexible
605 in its backbone torsion compared to aspartate, this mutation,
606 according to our hypothesis, will facilitate the attainment of
607 the partially open state transiting from the closed structure.
608 Another mutation, A570V, was observed within our predicted
609 residues, but did not yet become as widespread as D614G,
610 likely because it did not have substantial evolutionary advan-
611 tage. However, a different mutation at residue 570 (A570D),
612 has indeed appeared in the recently-emerged more-contagious
613 B.1.1.7 strain of SARS-CoV-2 (41). The consistency with
614 the mutation profile confirms that our dihedral-angle based
615 analysis can not only find out distant residues impacting RBD
616 dynamics, but can also predict residues where future mutations
617 can increase infection capability.

618 A cross-correlation metric based on linear mutual informa-
619 tion (LMI) was also employed to understand the long-distance
620 coupled motion between RBD and non-RBD residues. The
621 change in LMI correlation primarily takes place in the residues
622 adjacent to the RBD, but we could also distinctly observe long-
623 distance effects. Betweenness centrality (BC) of each residue
624 of the spike was computed from a C_{α} -based graph network
625 model for all three conformational states. The residues show-
626 ing largest changes in the BC are concentrated in NTD, RBD
627 and also in the linker regions joining the RBD with the rest
628 of the protein and also in the S2 domain. **Dynamic allostery**
629 **has been shown to impact the dynamics and consequently**
630 **the binding strength of ACE2 receptor and antibodies to the**
631 **mutated spike RBD (20). But significant change in centrality**
632 **measures of the non-RBD domains in our study suggests that**

RBD dynamics is also impacted by long-distance allosteric
effects within the spike protein itself; this emerges as a result of
the collective internal fluctuations of the amino-acid residues.

633 Experiments have not yet confirmed the role of S2 mutations
634 for RBD opening dynamics and for its binding affinity to
635 the ACE2 receptor. But whenever one observes a significant
636 change in infectivity or virulence in the newly emerging strains
637 of SARS CoV-2, it stems from a combined effect of multiple
638 mutations in the S1 and S2 domain. As our computational
639 approach has revealed that certain residues in the S2 domain
640 can potentially modify the propensity of the conformational
641 transition, the next logical step is to mutate those residues
642 only and observe the effect, which hopefully will be addressed
643 in future experimental studies. Moreover, the S2 domain is
644 also involved in the "tectonic" conformational rearrangement
645 required for the piercing of the host cell membrane (73), which
646 we, however, do not study in the current work.
647
648
649

650 Although our theoretical predictions of relevant residues,
651 connected to the changes in the RBD dynamics and effectively
652 leading to higher virulence, can seem somewhat speculative,
653 similar molecular dynamics studies on different proteins (74)
654 could reveal single key residues in hinge domain driving major
655 conformational changes, which subsequently have been con-
656 firmed by single-molecule experiments (75). We also point
657 out that our simulation of the wild-type spike can, by fiat,
658 only identify the residue to be mutated, but not the amino
659 acid to which the residue will be mutated to. However, both
660 experimental and computer simulation studies have already
661 established that D614G, A570D and a few other mutations
662 transform the dynamics of the RBD and favour an “up” state
663 (54, 55, 59, 61, 72). In the current work, we highlighted a set
664 of residues which show high correlation with RBD opening
665 motion. We refrain from performing additional simulations
666 by mutating those residues as our method cannot predict the
667 end result of the mutation, **and scanning over all possible**
668 **mutations would be computationally expensive. But we do**
669 **show that the dihedral angle preference, interaction energy**
670 **and hydrogen bonding pattern of concerned residues change**
671 **significantly due to a D614G mutation.** Furthermore, the topic
672 of whether the RBD opening motion increases infectivity can
673 only be resolved *in vivo*, given the complexity of the viral
674 entry process. A number of experiments and computational
675 studies indicated that binding to ACE2 is feasible only when
676 the RBD is “up” (27–31). This indicates that the down-to-up
677 conformational change is indeed necessary for binding to ACE2.
678 While we did not thoroughly study the dynamics of actual
679 mutant spike proteins, the role of specific point mutations in
680 the dynamics of RBD of the spike protein has been explored
681 using MD simulation in the literature. (60, 72)

682 From the point of view of immediate therapeutic interven-
683 tions, this study opens up the possibility of designing inhibitors
684 that bind to the regions outside the RBD, thereby preventing
685 infection by freezing RBD dynamics via steric restrictions on
686 specific distant residues. Such treatments are less likely to be
687 affected by the evolutionary adaptations in RBD sequence that
688 the virus performs frequently to evade the immune response.
689 In a starker context, future mutations in these key residues can
690 potentially change the infection rate and virulence, giving rise
691 to new strains and significantly altering the course of the pan-
692 demic. Our study and future work in this direction can make
693 the scientific community better prepared for such scenarios

694 and can help in efficient prevention of future outbreaks.

695 Data availability

696 The molecular dynamics trajectories are available from <http://doi.org/10.5281/zenodo.5052691>. The codes and the residue
697 correlation data used in this study are available from <https://github.com/dhimanray/COVID-19-correlation-work.git>. All further
698 details about the methods and the data are available within
699 the article and the SI Appendix.
700
701

702 Materials and Methods

703 The details of molecular dynamics simulations, tICA analysis, and
704 mutual information based network analysis are provided in the SI
705 Appendix. A brief outline is included below.

706 **System preparation and simulation details.** Glycosylated and sol-
707 vated structures of closed (PDB ID: 6VXX (32)) and partially
708 open (PDB ID: 6VSB (34)) spike head trimers were obtained from
709 the CHARMM-GUI COVID-19 archive (76). The glycans included
710 in the simulation are those from Table 1 of Ref (76). All simulations
711 were performed using the CHARMM36m force field (77). For the
712 purpose of the current work we considered residues 324-518 as the
713 RBD. After minimization and short equilibration, steered molecular
714 dynamics (SMD) simulation were performed to induce the opening
715 of the closed state and closing of the partially open state of the
716 RBD. Reaction coordinates (RC) were chosen to represent the dis-
717 tance of the RBD from its closed state position. Multiple structures
718 were chosen from the two SMD trajectories and two independent
719 umbrella sampling (US) simulations were performed for PDB ID:
720 6VXX and 6VSB. The reaction coordinate was restrained by a
721 harmonic potential with force constant of 1 kcal/mol/Å² for 35
722 windows and 26 windows for the two sets respectively. The colvars
723 module (78) was used for SMD and US calculations. Free energy
724 profiles were computed using weighted histogram analysis method
725 (WHAM) (79).

726 **Unbiased simulations.** Umbrella sampling trajectory frames were
727 sampled from the regions near the open, closed and the partially
728 open intermediate state judging the free energy value. Unbiased
729 simulations were performed starting from these frames, resulting
730 in 39 trajectories, each 40 ns long. Three of these trajectories
731 were identified as stable conformations corresponding to the closed,
732 partially open and fully open structure. These three trajectories
733 were extended to 80 ns. A cumulative ~ 1.7 μs unbiased simulation
734 data were generated and used in subsequent analysis. Additional 40
735 ns simulation was performed for the D614G mutant spike for each
736 of the closed and the partially open state. The structures of the
737 mutated species were generated using UCSF Chimera package (80).

738 **Time-lagged independent component analysis and mutual informa-**
739 **tion.** time-lagged independent component analysis (tICA) and prin-
740 cipal component analysis (PCA) were performed using pyEMMA
741 package (81) on the entire unbiased trajectory data. The feature
742 space for PCA and tICA consisted of pairwise distances between
743 specific residues in and around RBD of chain A and the NTD and
744 core domains.

745 The linear mutual information (LMI) based correlation was com-
746 puted for the closed, slightly open, partially open and fully open
747 state trajectories. A graph theory based network model was con-
748 structed with the C_α atom of each residue as node. The edge length
749 between nodes were computed from the cross correlation values
750 using previously described procedure (62). Betweenness centrality
751 of each residue was computed for each of the three trajectories and
752 compared. All the LMI and network analysis were performed using
753 bio3D package (82).

754 **Sequence alignment.** Iterative sequence alignment of the 67 strains
755 of SARS-CoV-2 spike protein sequences from the RCSB PDB
756 database was performed using the MAFFT-DASH program (83)
757 using the G-INS-i algorithm. The sequence of PDB ID: 6VXX was

used as the template. The alignment was analyzed with the ConSurf
server (84) to derive conservation scores for each residue position
in the alignment.

ACKNOWLEDGMENTS. This work was supported by the National
Science Foundation (NSF) via grant MCB 2028443. DR
acknowledges support by the Molecular Science Software Insti-
tute (MolSSI) seed COVID-19 fellowship funded by NSF via grant
number OAC-1547580. The authors thank Trevor Gokey for a stim-
ulating discussion. The work has benefited from the computational
resources of the UC Irvine High Performance Computing (HPC)
cluster.

1. P Zhou, et al., A pneumonia outbreak associated with a new coronavirus of probable bat origin. *Nature* **579**, 270–273 (2020).
2. R Lu, et al., Genomic characterisation and epidemiology of 2019 novel coronavirus: implications for virus origins and receptor binding. *The Lancet* **395**, 565–574 (2020).
3. X Ou, et al., Characterization of spike glycoprotein of SARS-CoV-2 on virus entry and its immune cross-reactivity with SARS-CoV. *Nat. Commun.* **11**, 1–12 (2020).
4. W Tai, et al., Characterization of the receptor-binding domain (RBD) of 2019 novel coronavirus: implication for development of RBD protein as a viral attachment inhibitor and vaccine. *Cell. Mol. Immunol.* **17**, 613–620 (2020).
5. T Koyama, D Platt, L Parida, Variant analysis of SARS-cov-2 genomes. *Bull. World Heal. Organ.* **98**, 495 (2020).
6. KM Peck, AS Lauring, Complexities of viral mutation rates. *J. virology* **92** (2018).
7. Z Zhao, et al., Moderate mutation rate in the SARS coronavirus genome and its implications. *BMC Evol. Biol.* **4**, 21 (2004).
8. L van Dorp, et al., Emergence of genomic diversity and recurrent mutations in sars-cov-2. *Infect. Genet. Evol.* **83**, 104351 (2020).
9. N Kaushal, et al., Mutational frequencies of SARS-CoV-2 genome during the beginning months of the outbreak in USA. *Pathogens* **9**, 565 (2020).
10. S Laha, et al., Characterizations of sars-cov-2 mutational profile, spike protein stability and viral transmission. *Infect. Genet. Evol.* **85**, 104445 (2020).
11. S Isabel, et al., Evolutionary and structural analyses of SARS-CoV-2 D614G spike protein mutation now documented worldwide. *Sci. Reports* **10**, 14031 (2020).
12. TF Rogers, et al., Isolation of potent SARS-CoV-2 neutralizing antibodies and protection from disease in a small animal model. *Science* **369**, 956–963 (2020).
13. W Li, et al., Rapid identification of a human antibody with high prophylactic and therapeutic efficacy in three animal models of sars-cov-2 infection. *Proc. Natl. Acad. Sci.* **117**, 29832–29838 (2020).
14. SJ Zost, et al., Potently neutralizing and protective human antibodies against SARS-CoV-2. *Nature* **584**, 443–449 (2020).
15. S Jiang, X Zhang, L Du, Therapeutic antibodies and fusion inhibitors targeting the spike protein of sars-cov-2. *Expert. Opin. on Ther. Targets* **0**, 1–7 (2020) PMID: 32941780.
16. M Smith, JC Smith, Repurposing therapeutics for covid-19: Supercomputer-based docking to the sars-cov-2 viral spike protein and viral spike protein-human ace2 interface. *ChemRxiv* (2020).
17. R Chowdhury, V Sai Sreyas Adury, A Vijay, RK Singh, A Mukherjee, Atomistic de-novo inhibitor generation-guided drug repurposing for sars-cov-2 spike protein with free-energy validation by well-tempered metadynamics. *Chem. Asian J.* **16**, 1634–1642 (2021).
18. Y Han, P Král, Computational design of ace2-based peptide inhibitors of sars-cov-2. *ACS Nano* **14**, 5143–5147 (2020) PMID: 32286790.
19. GM Verkhivker, Molecular simulations and network modeling reveal an allosteric signaling in the sars-cov-2 spike proteins. *J. proteome research* **19**, 4587–4608 (2020).
20. A Spinello, A Saitalamacchia, J Borišek, A Magistrato, Allosteric cross-talk among spike's receptor-binding domain mutations of the sars-cov-2 south african variant triggers an effective hijacking of human cell receptor. *The J. Phys. Chem. Lett.* **0**, 5987–5993 (2021) PMID: 34161095.
21. AJ Greaney, et al., Comprehensive mapping of mutations in the sars-cov-2 receptor-binding domain that affect recognition by polyclonal human plasma antibodies. *Cell host & microbe* **29**, 463–476 (2021).
22. L Liu, et al., Potent neutralizing antibodies against multiple epitopes on sars-cov-2 spike. *Nature* **584**, 450–456 (2020).
23. KW Ng, et al., Preexisting and de novo humoral immunity to sars-cov-2 in humans. *Science* **370**, 1339–1343 (2020).
24. L Di Paola, H Hadi-Aljanvand, X Song, G Hu, A Giuliani, The discovery of a putative allosteric site in the sars-cov-2 spike protein using an integrated structural/dynamic approach. *J. proteome research* **19**, 4576–4586 (2020).
25. FA Olotu, KF Omolabi, ME Soliman, Leaving no stone unturned: Allosteric targeting of sars-cov-2 spike protein at putative druggable sites disrupts human angiotensin-converting enzyme interactions at the receptor binding domain. *Informatics medicine unlocked* **21**, 100451 (2020).
26. PV Raghuvamsi, et al., Sars-cov-2 s protein: Ace2 interaction reveals novel allosteric targets. *Elife* **10**, e63646 (2021).
27. J Shang, et al., Cell entry mechanisms of sars-cov-2. *Proc. Natl. Acad. Sci.* **117**, 11727–11734 (2020).
28. M Gui, et al., Cryo-electron microscopy structures of the sars-cov spike glycoprotein reveal a prerequisite conformational state for receptor binding. *Cell research* **27**, 119–129 (2017).
29. Y Yuan, et al., Cryo-em structures of mers-cov and sars-cov spike glycoproteins reveal the dynamic receptor binding domains. *Nat. communications* **8**, 1–9 (2017).
30. M Gur, et al., Conformational transition of sars-cov-2 spike glycoprotein between its closed and open states. *The J. Chem. Phys.* **153**, 075101 (2020).

- 838 31. C Peng, et al., Computational study of the strong binding mechanism of sars-cov-2 spike and
839 ace2. *ChemRxiv Prepr.* **10** (2020).
- 840 32. AC Walls, et al., Structure, function, and antigenicity of the sars-cov-2 spike glycoprotein. *Cell*
841 **181**, 281–292.e6 (2020).
- 842 33. Y Cai, et al., Distinct conformational states of sars-cov-2 spike protein. *Science* **369**, 1586–
843 1592 (2020).
- 844 34. D Wrapp, et al., Cryo-em structure of the 2019-ncov spike in the prefusion conformation.
845 *Science* **367**, 1260–1263 (2020).
- 846 35. L Casalino, et al., Beyond shielding: The roles of glycans in the sars-cov-2 spike protein. *ACS*
847 *Cent. Sci.* **6**, 1722–1734 (2020).
- 848 36. MI Zimmerman, et al., Sars-cov-2 simulations go exascale to predict dramatic spike opening
849 and cryptic pockets across the proteome. *Nat. Chem.* **13**, 651–659 (2021).
- 850 37. S Roy, A Jaiswar, R Sarkar, Dynamic asymmetry exposes 2019-ncov prefusion spike. *The*
851 *journal physical chemistry letters* **11**, 7021–7027 (2020).
- 852 38. T Sztain, et al., A glycan gate controls opening of the sars-cov-2 spike protein. *bioRxiv*
853 (2021).
- 854 39. C Bustamante, L Alexander, K Maciuba, CM Kaiser, Single-molecule studies of protein folding
855 with optical tweezers. *Annu. review biochemistry* **89**, 443–470 (2020).
- 856 40. B Korber, et al., Tracking changes in sars-cov-2 spike: Evidence that d614g increases infec-
857 tivity of the covid-19 virus. *Cell* **182**, 812–827.e19 (2020).
- 858 41. A Rambaut, et al., Preliminary genomic characterisation of an emergent SARS-CoV-2 lineage
859 in the UK defined by a novel set of spike mutations, Technical report (2020).
- 860 42. I Jolliffe, *Principal Component Analysis*. (Springer-Verlag, New York), 2 edition, p. 488 (2002).
- 861 43. L Molgedey, HG Schuster, Separation of a mixture of independent signals using time delayed
862 correlations. *Phys. Rev. Lett.* **72**, 3634–3637 (1994).
- 863 44. G Pérez-Hernández, F Paul, T Giorgino, G De Fabritiis, F Noé, Identification of slow molecular
864 order parameters for Markov model construction. *The J. Chem. Phys.* **139**, 015102 (2013).
- 865 45. CR Schwantes, VS Pande, Improvements in markov state model construction reveal many
866 non-native interactions in the folding of nt19. *J. Chem. Theory Comput.* **9**, 2000–2009 (2013).
- 867 46. LS Caves, JD Evanseck, M Karplus, Locally accessible conformations of proteins: Multiple
868 molecular dynamics simulations of crambin. *Protein Sci.* **7**, 649–666 (1998).
- 869 47. I Echeverria, DE Makarov, GA Papoian, Concerted dihedral rotations give rise to internal
870 friction in unfolded proteins. *J. Am. Chem. Soc.* **136**, 8708–8713 (2014).
- 871 48. C Levinthal, How to fold graciously. *Mossbauer spectroscopy biological systems* **67**, 22–24
872 (1969).
- 873 49. JP Eckmann, D Ruelle, Ergodic theory of chaos and strange attractors. *Rev. Mod. Phys.* **57**,
874 617–656 (1985).
- 875 50. AR Fadel, DQ Jin, GT Montelione, RM Levy, Crankshaft motions of the polypeptide backbone
876 in molecular dynamics simulations of human type- α transforming growth factor. *J. biomolec-*
877 *ular NMR* **6**, 221–226 (1995).
- 878 51. L Fallon, et al., Free energy landscapes from sars-cov-2 spike glycoprotein simulations sug-
879 gest that rbd opening can be modulated via interactions in an allosteric pocket. *J. Am. Chem.*
880 *Soc.* **XXXX**, XXX–XXX (2021).
- 881 52. MM Sauer, et al., Structural basis for broad coronavirus neutralization. *Nat. Struct. & Mol.*
882 *Biol.* **28**, 478–486 (2021).
- 883 53. R Nachbagauer, et al., A chimeric hemagglutinin-based universal influenza virus vaccine ap-
884 proach induces broad and long-lasting immunity in a randomized, placebo-controlled phase i
885 trial. *Nat. Medicine* **27**, 106–114 (2021).
- 886 54. L Yurkovetskiy, et al., Structural and functional analysis of the d614g sars-cov-2 spike protein
887 variant. *Cell* **183**, 739–751 (2020).
- 888 55. SMC Gobeil, et al., D614g mutation alters sars-cov-2 spike conformation and enhances pro-
889 tease cleavage at the s1/s2 junction. *Cell reports* **34**, 108630 (2021).
- 890 56. J Schymkowitz, et al., The FoldX web server: an online force field. *Nucleic Acids Res.* **33**,
891 W382–W388 (2005).
- 892 57. Rapid increase of a SARS-CoV-2 variant with multiple spike protein mutations observed in
893 the United Kingdom (2020).
- 894 58. B Meng, et al., Recurrent emergence of sars-cov-2 spike deletion h69/v70 and its role in the
895 alpha variant b. 1.1. 7. *Cell reports* **35**, 109292 (2021).
- 896 59. R Henderson, et al., Controlling the sars-cov-2 spike glycoprotein conformation. *Nat. struc-*
897 *tural & molecular biology* **27**, 925–933 (2020).
- 898 60. GM Verkhivker, L Di Paola, Dynamic network modeling of allosteric interactions and com-
899 munication pathways in the sars-cov-2 spike trimer mutants: Differential modulation of conforma-
900 tional landscapes and signal transmission via cascades of regulatory switches. *The J. Phys.*
901 *Chem. B* **125**, 850–873 (2021).
- 902 61. RA Mansbach, et al., The sars-cov-2 spike variant d614g favors an open conformational state.
903 *Sci. advances* **7**, eabf3671 (2021).
- 904 62. I Rivalta, et al., Allosteric pathways in imidazole glycerol phosphate synthase. *Proc. Natl.*
905 *Acad. Sci.* **109**, E1428–E1436 (2012).
- 906 63. CF Negre, et al., Eigenvector centrality for characterization of protein allosteric pathways.
907 *Proc. Natl. Acad. Sci.* **115**, E12201–E12208 (2018).
- 908 64. CL McClendon, G Friedland, DL Mobley, H Amirkhani, MP Jacobson, Quantifying correlations
909 between allosteric sites in thermodynamic ensembles. *J. chemical theory computation* **5**,
910 2486–2502 (2009).
- 911 65. CL McClendon, AP Kornev, MK Gilson, SS Taylor, Dynamic architecture of a protein kinase.
912 *Proc. Natl. Acad. Sci.* **111**, E4623–E4631 (2014).
- 913 66. LG Ahuja, PC Aoto, AP Kornev, G Veglia, SS Taylor, Dynamic allostery-based molecular
914 workings of kinase: peptide complexes. *Proc. Natl. Acad. Sci.* **116**, 15052–15061 (2019).
- 915 67. S Bowerman, J Wereszczynski, Detecting allosteric networks using molecular dynamics sim-
916 ulation. *Methods Enzymol.* **578**, 429–447 (2016).
- 917 68. T Ichiye, M Karplus, Collective motions in proteins: a covariance analysis of atomic fluctu-
918 ations in molecular dynamics and normal mode simulations. *Proteins: Struct. Funct. Bioin-*
919 *forma.* **11**, 205–217 (1991).
- 920 69. OF Lange, H Grubmüller, Generalized correlation for biomolecular dynamics. *Proteins: Struct.*
921 *Funct. Bioinforma.* **62**, 1053–1061 (2006).
70. N Ota, DA Agard, Intramolecular signaling pathways revealed by modeling anisotropic ther-
922 mal diffusion. *J. molecular biology* **351**, 345–354 (2005).
- 923 71. A Saltalamacchia, et al., Decrypting the information exchange pathways across the spliceo-
924 some machinery. *J. Am. Chem. Soc.* **142**, 8403–8411 (2020).
- 925 72. GM Verkhivker, S Agajanian, D Oztas, G Gupta, Computational analysis of protein stability
926 and allosteric interaction networks in distinct conformational forms of the sars-cov-2 spike
927 d614g mutant: reconciling functional mechanisms through allosteric model of spike regulation.
928 *J. Biomol. Struct. Dyn.* **0**, 1–18 (2021) PMID: 34060425.
- 929 73. AC Walls, et al., Tectonic conformational changes of a coronavirus spike glycoprotein promote
930 membrane fusion. *Proc. Natl. Acad. Sci.* **114**, 11157–11162 (2017).
- 931 74. J Wereszczynski, I Andricioaei, Free energy calculations reveal rotating-ratchet mechanism
932 for dna supercoil relaxation by topoisomerase II and its inhibition. *Biophys. Journal* **99**, 869–
933 878 (2010).
- 934 75. Y Seol, H Zhang, Y Pommier, KC Neuman, A kinetic clutch governs religation by type II
935 topoisomerases and determines camptothecin sensitivity. *Proc. Natl. Acad. Sci.* **109**, 16125–
936 16130 (2012).
- 937 76. H Woo, et al., Developing a fully glycosylated full-length sars-cov-2 spike protein model in a
938 viral membrane. *The J. Phys. Chem. B* **124**, 7128–7137 (2020) PMID: 32559081.
- 939 77. J Huang, et al., CHARMM36m: an improved force field for folded and intrinsically disordered
940 proteins. *Nat. Methods* **14**, 71–73 (2017).
- 941 78. G Fiorin, ML Klein, J Hénin, Using collective variables to drive molecular dynamics simula-
942 tions. *Mol. Phys.* **111**, 3345–3362 (2013).
- 943 79. B Roux, The calculation of the potential of mean force using computer simulations. *Comput.*
944 *Phys. Commun.* **91**, 275–282 (1995).
- 945 80. EF Pettersen, et al., Ucsf chimera—a visualization system for exploratory research and anal-
946 ysis. *J. computational chemistry* **25**, 1605–1612 (2004).
- 947 81. MK Scherer, et al., PyEMMA 2: A Software Package for Estimation, Validation, and Analysis
948 of Markov Models. *J. Chem. Theory Comput.* **11**, 5525–5542 (2015).
- 949 82. BJ Grant, AP Rodrigues, KM EISawy, JA McCammon, LS Caves, Bio3d: an r package for the
950 comparative analysis of protein structures. *Bioinformatics* **22**, 2695–2696 (2006).
- 951 83. J Rozewicki, S Li, KM Amada, DM Standley, K Katoh, Mafft-dash: integrated protein se-
952 quence and structural alignment. *Nucleic acids research* **47**, W5–W10 (2019).
- 953 84. H Ashkenazy, et al., ConSurf 2016: an improved methodology to estimate and visualize evo-
954 lutionary conservation in macromolecules. *Nucleic acids research* **44**, W344–W350 (2016).
- 955